Available online at www.sciencedirect.com
SCIENCE DIRECT®
International Journal of Heat and Mass Transfer 48 (2005) 3018–3033
International Journal of HEAT and MASS TRANSFER
www.elsevier.com/locate/ijhmt

Two-dimensional thermal analysis of a polygonal fin with two tubes on a square pitch

L. Marin [a,*], L. Elliott [b], P.J. Heggs [c], D.B. Ingham [b], D. Lesnic [b], X. Wen [a]

[a] School of Earth and Environment, Environment Centre, University of Leeds, Leeds LS2 9JT, UK
[b] Department of Applied Mathematics, University of Leeds, Leeds LS2 9JT, UK
[c] Department of Chemical Engineering, University of Manchester, P.O. Box 88, Manchester M60 1QD, UK

Received 2 April 2004
Available online 14 April 2005

Abstract

The boundary element method (BEM) has been used to investigate the two-dimensional temperature distribution and the flow of heat from a polygonal fin with two tubes on a square pitch. This numerical method is shown to be convergent, stable and consistent. The resultant heat flows from the fin and the tubes are presented in the form of fin performance ratios. The values of the two-dimensional fin performance ratios are almost identical to those obtained for a single radial rectangular fin of equivalent surface area. The one-dimensional fin performance indicators, fin performance ratio or fin efficiency can be used to predict the heat flows. However, the two-dimensional temperature distributions have revealed the existence of conductive paths between the two tubes depending upon the fin dimensions, the values of the heat transfer and material thermal conductivity, and the magnitude of the temperature differences between the two tubes and the surrounding air.

Keywords: Polygonal fins; Fin performance indicators; Heat flows; Temperature distributions; Conductive paths; Boundary element method

1. Introduction

Heat exchangers (evaporators and condensers) are integral parts of vapour-compression refrigeration systems. Many of these heat exchangers employ extended surfaces on the air side comprising spaced thin metal sheets (normally either 0.2 mm or 0.4 mm thick) with tubes passing through each sheet. In these exchangers the evaporation or condensation occurs within the tubes and air flows between the sheets and over the tubes. The film heat transfer coefficient on the air side is normally two orders of magnitude smaller than the condensing or evaporating coefficients and without the extended surface arrangement would dominate the overall coefficient and result in very large units. The metal sheets provide considerable extra area on the air side and hence the combined film coefficient and additional area reduce the air side thermal resistance so that much larger overall heat coefficients are obtained and thus smaller exchangers may be employed. The sheets are mechanically stamped to produce a regular array of circular holes in

* Corresponding author. Present address: School of Mechanical, Material, Manufacturing Engineering and Management, The University of Nottingham, University Park, Nottingham NG7 2RD, UK. Tel.: +44 (0)115 8467683; fax: +44 (0)115 9513800.
E-mail address: liviu.marin@nottingham.ac.uk (L. Marin).

0017-9310/$ - see front matter © 2005 Elsevier Ltd. All rights reserved.
doi:10.1016/j.ijheatmasstransfer.2004.11.030

Nomenclature

$\boldsymbol{A}, \boldsymbol{B}, \boldsymbol{C}$ matrices corresponding to the boundary element discretisation
Bi transverse Biot number
err(PR) relative percentage error in evaluating the fin performance ratio
E fundamental solution for the modified Helmholtz equation
$\boldsymbol{f}$ right-hand side vector of the discretised system
$H_0^{(1)}$ Hankel function of the first kind of order zero
I_0 modified Bessel function of the first kind of order zero
I_1 modified Bessel function of the first kind of order one
K_0 modified Bessel function of the second kind of order zero
K_1 modified Bessel function of the second kind of order one
l length of the equivalent radial rectangular fin [m]
$l^{(s)}$ length of the square rectangular fin [m]
$L^{(s)}$ length of the non-dimensionalised square fin
N, N_{i1}, N_{i2}, N_0 numbers of boundary elements
PR fin performance ratio
$\dot{Q}$ heat flow if the fin was not attached to the primary surface [W]
$\dot{Q}_f$ heat flow through the fin [W]
$\dot{Q}_f^{(1)}, \dot{Q}_f^{(2)}$ calculated heat flows through the fin [W]
$\dot{Q}_{f,max}$ maximum possible heat flow through the fin [W]
$r(\underline{X}, \underline{Y})$ distance between the load point $\underline{X}$ and the field point $\underline{Y}$
r_i inner radius of the fin (outer radius of the tube) [m]
$r_o^{(r)}$ outer radius of the equivalent radial rectangular fin [m]
$r_o^{(s)}$ radius of the circle which encloses the square fin [m]
R_i inner radius of the non-dimensionalised fin
$R_o^{(r)}$ outer radius of the equivalent non-dimensionalised radial rectangular fin
$R_o^{(s)}$ radius of the circle which encloses the non-dimensionalised square fin
$\mathbb{R}$ real number set
T_b^1, T_b^2 fin base (tube) temperatures [°C]
T_f fin temperature [°C]
T_∞ ambient medium temperature [°C]
$\boldsymbol{x}$ vector containing the unknown boundary values of the non-dimensional temperature and flux at the collocation points
$\underline{x}, \underline{y}, \underline{X}, \underline{Y}$ space variables
$\underline{X}^m$ collocation point/node
$\underline{Y_{i1}}^{n-1}, \underline{Y_{i1}}^n$ endpoints of the boundary element $\widetilde{\Gamma}_{1i}^{(n)}$
$\underline{Y_{i2}}^{n-1}, \underline{Y_{i2}}^n$ endpoints of the boundary element $\widetilde{\Gamma}_{2i}^{(n)}$
$\underline{Y_o}^{n-1}, \underline{Y_o}^n$ endpoints of the boundary element $\widetilde{\Gamma}_o^{(n)}$

Greek symbols

α convective heat transfer coefficient [W m^{-2} K^{-1}]
δ_f half-fin thickness [m]
δ_{mn} Kronecker delta symbol
η_f fin efficiency
$\boldsymbol{\varphi}$ vector containing the discretised non-dimensional boundary flux
$\emptyset$ empty set
$\partial\Omega$ boundary of the solution domain Ω
$\partial\widetilde{\Omega}$ boundary of the non-dimensionalised solution domain $\widetilde{\Omega}$
$\Gamma_{i1}, \Gamma_{i2}, \Gamma_o$ parts of the boundary of the solution domain Ω
$\widetilde{\Gamma}_{i1}, \widetilde{\Gamma}_{i2}, \widetilde{\Gamma}_o$ parts of the boundary of the non-dimensionalised solution domain $\widetilde{\Omega}$
$\widetilde{\Gamma}_{i1}^{(n)}, \widetilde{\Gamma}_{i2}^{(n)}, \widetilde{\Gamma}_o^{(n)}, \widetilde{\Gamma}_n$ boundary elements
λ_f thermal conductivity of the fin [W m^{-1} K^{-1}]
$\underline{\nu}$ unit outward normal vector to the boundary Γ_o
$\underline{\widetilde{\nu}}$ unit outward normal vector to the boundary $\widetilde{\Gamma}_o$
Ω solution domain
$\widetilde{\Omega}$ non-dimensionalised solution domain
$\boldsymbol{\theta}$ vector containing the discretised non-dimensional boundary temperature
θ_f non-dimensional fin temperature
ζ_f fin effectiveness
ζ_{max} maximum fin effectiveness

Subscripts

m m component of a vector
nm (n, m) component of a second-order tensor

Superscripts

an analytical value
num numerical value

either square or hexagonal arrangements. The excess metal forms a predetermined rim, which results in the spacing between adjacent sheets in the heat exchangers. The sheets are automatically fed onto the set of tubes to create the heat exchanger block. Finally, the tubes are mechanically expanded to provide intimate contact

between the tubes, the rims and the sheet. To complete the heat exchanger, U bends are attached to the ends of adjacent tubes in the block so that various flow paths arrangements for the refrigerant within the tubes can be obtained, see Fig. 1. Each sheet in the final heat exchanger results in the so-called polygonal fin assembly, see Marin et al. [1] and Kraus et al. [2]. Unlike many other types of extended surfaces, the polygonal fin assembly results in direct conductive paths between the tubes passing through the sheet.

Unfortunately, all the sheet area is not fully utilised, because the temperature difference between the sheet and the air falls progressively from the base of the fin (tube outer surface) to the outer regions of the fin geometry. Design methods employ fin performance indicators (fin efficiency [2–4], fin effectiveness [5] and more recently, fin performance ratio [6]) to accommodate this phenomenon of under-utilisation of the additional area in the evaluation of the thermal resistance on the air side. Fin performance indicators that allow for the two-dimensional temperature distributions within polygonal fins do not exist and designers must resort to approximate techniques. However, these techniques do not attempt to consider the two-dimensionality (radial and angular) of the heat flow and the presence of other tubes in the assembly.

The theory of heat flow along fins attached to a primary surface at one end only has been thoroughly investigated, see e.g. the pioneering work of Harper and Brown [7] and the classical book of Kraus et al. [2]. However, the analysis of fin problems is conventionally based on the assumption that the heat flow is uni-directional because this fact, in general, facilitates an analytical treatment, see e.g. Gardner [3,4] and Mikk [8]. The early investigations into the applicability of the one-dimensional approximation restricted attention solely to the fin and concluded that two-dimensional effects are negligible provided that the transverse Biot number ($Bi = \alpha\delta_f/\lambda_f$) is much less than unity, see Irey [9], Levitsky [10] and Lau and Tan [11]. However, later investigations of the combined fin and supporting surface, see e.g. Sparrow and Lee [12], Suryanarayana [13] and Heggs and Stones [14], have shown that the presence of fins induces transverse two-dimensional effects within the supporting surface and these may in turn act to produce two-dimensional variations within the fin. However, the two-dimensional transverse effects were found to occur only in long fins, when the coupled wall and fin models were investigated. The previous investigators have only considered the two-dimensional effects in a single fin with the base held at a fixed temperature. This lead to the conclusion that two-dimensional effects occur in short fins, whereas they occur near the base of very long fins and for these fins, the heat flow through the wall will be relatively large.

For polygonal fin assemblies, the relative length of the fins is short and so transverse conduction effects can be ignored. However, it is essential that multi-dimensional analysis in the other two directions of the fin surface is considered when developing performance indicators for the effective design of heat exchangers. Suryanarayana [13] has reported that the difference between heat transfer rates can be as much as 80%. It is therefore essential for the effective design of heat exchangers using polygonal fin assemblies to employ a multi-dimensional analysis.

In this paper, we extend the study of a single isolated polygonal fin on hexagonal and square pitches performed by Marin et al. [1] to the case of two tubes at different temperatures passing through a rectangular fin, see Fig. 2 which shows a photograph of polygonal fin heat exchanger blocks with one and two tubes on a square pitch produced by Elfin Technology Ltd. In the previous study for the single isolated polygonal fin, it was demonstrated that the two-dimensional temperature distribution in square and hexagonal fins, and the resulting heat flow from the fins, could be predicted by a one-

Fig. 1. Photograph of a fin exchanger block.

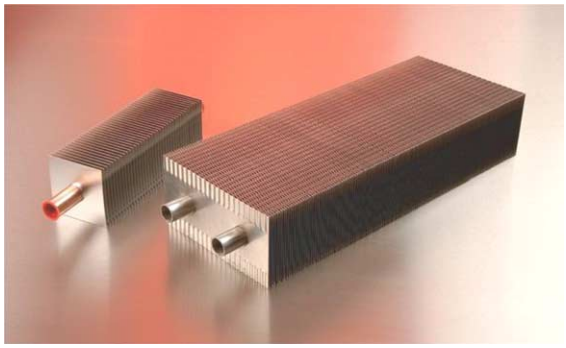

Fig. 2. Photograph of polygonal fin heat exchanger blocks with one and two tubes on a square pitch produced by Elfin Technology Ltd.

dimensional radial rectangular fin with the equivalent surface area of the polygonal fins. Consequently, the conduction/convection problem for square fin assemblies is solved numerically by employing a convergent, stable and consistent two-dimensional boundary element method (BEM) based algorithm. The performance of a particular heat exchanger for which detailed experimental data is available [18] is predicted and compared in the normal energy procedure taking the equivalent radial fin with an adiabatic condition on the outer radius. Moreover, the isotherms corresponding to the geometry under investigation are also presented.

2. Mathematical formulation

From a geometrical point of view, square fins are characterised by the inner radius (the outer radius of the tube), r_i, the radius of the circle which encloses the square fin, $r_o^{(s)}$, the fin length, $l^{(s)} = r_o^{(s)} - r_i$, see Fig. 3, and the half-fin thickness, δ_f. We also consider the corresponding equivalent radial rectangular fin which has the same surface area, inner radius and thickness as the square fin under investigation, the outer radius, $r_o^{(r)}$, such that $r_o^{(r)} = \sqrt{2/\pi} r_o^{(s)}$, and the fin length $l = r_o^{(r)} - r_i$.

In this study, we restrict ourselves to a polygonal fin assembly consisting of two neighbouring tubes on a square pitch arrangement. The theoretical model is based on the following assumptions which are commonly made for the analysis of fin heat transfer regardless of the fin assembly geometry, see [2–4,15],

(i) The heat transfer through the fin assembly is at steady state and, in addition, there is no heat generation in the fin material.

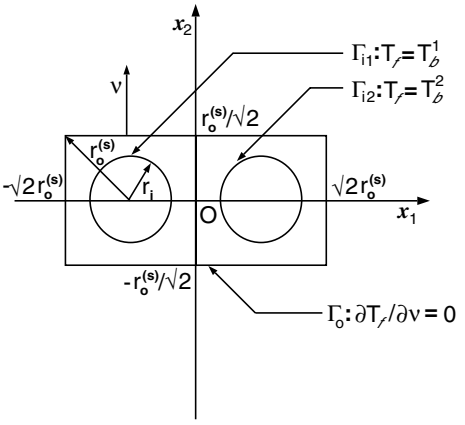

Fig. 3. Sketch of the polygonal fin assembly under investigation.

(ii) The fin assembly transfers heat to the ambient medium solely due to convection and the coefficient of convective heat transfer, α, is uniform over the entire fin assembly surface.
(iii) The temperature of the ambient medium, T_∞, is uniform and constant over the fin assembly surface.
(iv) The material is of constant thermal conductivity, λ_f.
(v) The surface temperatures of the tubes, $T_b^1 \geqslant T_b^2$, are constant.
(vi) Based on the thin fin assumption, the temperature variation in the fin assembly normal to its surface is neglected.

Let $\Omega = (-\sqrt{2}r_o^{(s)}, \sqrt{2}r_o^{(s)}) \times (-r_o^{(s)}/\sqrt{2}, r_o^{(s)}/\sqrt{2}) \setminus (\Omega_{i1} \cup \Omega_{i2}) \subset \mathbb{R}^2$ be the two-dimensional open bounded domain occupied by the square fin assembly under investigation, where $\Omega_{i1} = \{\underline{x} = (x_1, x_2) \mid (x_1 - r_o^{(s)}/\sqrt{2})^2 + x_2^2 \leqslant r_i^2\}$ and $\Omega_{i2} = \{\underline{x} = (x_1, x_2) \mid (x_1 + r_o^{(s)}/\sqrt{2})^2 + x_2^2 \leqslant r_i^2\}$ are the domains occupied by the tubes, with the boundary $\partial\Omega = \Gamma_{i1} \cup \Gamma_{i2} \cup \Gamma_o$, $\Gamma_{i1} \cap \Gamma_o = \Gamma_{i2} \cap \Gamma_o = \Gamma_{i1} \cap \Gamma_{i2} = \emptyset$, $\Gamma_{i1} = \partial\Omega_{i1}$, $\Gamma_{i2} = \partial\Omega_{i2}$ and $\Gamma_o = \{\pm\sqrt{2}r_o^{(s)}\} \times (-r_o^{(s)}/\sqrt{2}, r_o^{(s)}/\sqrt{2}) \cup (-\sqrt{2}r_o^{(s)}, \sqrt{2}r_o^{(s)}) \times \{\pm r_o^{(s)}/\sqrt{2}\}$.

The governing partial differential equation for the two-dimensional temperature distribution $T_f(\underline{x})$ can be derived as follows:

$$\frac{\partial^2 T_f(\underline{x})}{\partial x_1^2} + \frac{\partial^2 T_f(\underline{x})}{\partial x_2^2} - \frac{\alpha}{\lambda_f \delta_f}(T_f(\underline{x}) - T_\infty) = 0, \quad \underline{x} \in \Omega. \tag{1}$$

The boundary conditions for the two-dimensional fin assembly temperature are given by isothermal conditions at the base of each square fin, Γ_{i1} and Γ_{i2},

$$T_f(\underline{x}) = \begin{cases} T_b^1, & \underline{x} \in \Gamma_{i1}, \\ T_b^2, & \underline{x} \in \Gamma_{i2}, \end{cases} \quad T_b^1 \geqslant T_b^2, \tag{2}$$

and at the tip of the fin assembly, Γ_o, by assuming the heat transfer from the fin assembly tip to the surrounding ambient medium to be negligible (adiabatic condition) due to its very small thickness

$$\frac{\partial T_f(\underline{x})}{\partial \nu} = 0, \quad \underline{x} \in \Gamma_o, \tag{3}$$

where $\nu(\underline{x})$ is the outward normal vector at the boundary Γ_o.

On introducing the following dimensionless variables and parameters, see [1,5,16]:

$$X_j = \frac{1}{\zeta_{max}}\left(\frac{x_j}{\delta_f}\right), \quad j = 1, 2, \quad \zeta_{max} = \sqrt{\frac{\lambda_f}{\alpha\delta_f}}, \tag{4}$$
$$\theta_f(\underline{X}) = (T_f(\underline{x}) - T_\infty)/(T_b^1 - T_\infty),$$

the governing partial differential equation (1) and the boundary conditions (2) and (3) can be recast in non-dimensional and homogeneous form as follows:

$$\frac{\partial^2\theta_f(\underline{X})}{\partial X_1^2}+\frac{\partial^2\theta_f(\underline{X})}{\partial X_2^2}-\theta_f(\underline{X})=0,\quad \underline{X}\in\widetilde{\Omega}, \tag{5}$$

$$\theta_f(\underline{X})=\begin{cases}1, & \underline{X}\in\widetilde{\Gamma}_{i1},\\ (T_b^2-T_\infty)/(T_b^1-T_\infty)\leqslant 1, & \underline{X}\in\widetilde{\Gamma}_{i2},\end{cases} \tag{6}$$

$$\frac{\partial\theta_f(\underline{X})}{\partial\tilde{v}}=0,\quad \underline{X}\in\widetilde{\Gamma}_o. \tag{7}$$

Here $\widetilde{\Omega}$, $\widetilde{\Omega}_{i1}$, $\widetilde{\Omega}_{i2}$, $\widetilde{\Gamma}_{i1}$, $\widetilde{\Gamma}_{i2}$, $\widetilde{\Gamma}_o$ and $\tilde{v}$ are the transformed domains Ω, Ω_{i1} and Ω_{i2}, inner boundaries Γ_{i1} and Γ_{i2}, outer boundary Γ_o and outward normal v at the boundary Γ_o, respectively, obtained using the change of variables given by Eq. (4), i.e.

$$\widetilde{\Omega}=\left(-\sqrt{2}R_o^{(s)},\sqrt{2}R_o^{(s)}\right)\times\left(-R_o^{(s)}/\sqrt{2},R_o^{(s)}/\sqrt{2}\right)\Big\backslash\left(\widetilde{\Omega}_{i1}\cup\widetilde{\Omega}_{i2}\right)\subset\mathbb{R}^2, \tag{8}$$

$$\widetilde{\Omega}_{i1}=\left\{\underline{X}=(X_1,X_2)\,\middle|\,\left(X_1-R_o^{(s)}/\sqrt{2}\right)^2+X_2^2\leqslant R_i^2\right\}, \tag{9}$$

$$\widetilde{\Omega}_{i2}=\left\{\underline{X}=(X_1,X_2)\,\middle|\,\left(X_1+R_o^{(s)}/\sqrt{2}\right)^2+X_2^2\leqslant R_i^2\right\}, \tag{10}$$

$$\partial\widetilde{\Omega}=\widetilde{\Gamma}_{i1}\cup\widetilde{\Gamma}_{i2}\cup\widetilde{\Gamma}_o,\quad \widetilde{\Gamma}_{i1}\cap\widetilde{\Gamma}_o=\widetilde{\Gamma}_{i2}\cap\widetilde{\Gamma}_o=\widetilde{\Gamma}_{i1}\cap\widetilde{\Gamma}_{i2}=\emptyset,\quad \widetilde{\Gamma}_{i1}=\partial\widetilde{\Omega}_{i1},\quad \widetilde{\Gamma}_{i2}=\partial\widetilde{\Omega}_{i2}, \tag{11}$$

$$\widetilde{\Gamma}_o=\left\{\pm\sqrt{2}R_o^{(s)}\right\}\times\left(-R_o^{(s)}/\sqrt{2},R_o^{(s)}/\sqrt{2}\right)\cup\left(-\sqrt{2}R_o^{(s)},\sqrt{2}R_o^{(s)}\right)\times\left\{\pm R_o^{(s)}/\sqrt{2}\right\}, \tag{12}$$

$$R_o^{(s)}=r_o^{(s)}/(\delta_f\zeta_{max}),\quad R_i=r_i/(\delta_f\zeta_{max}). \tag{13}$$

It should be mentioned that the non-dimensional variables X_j and θ_f, as well as the dimensionless parameters ζ_{max} and x_j/δ_f, given by relation (4) occur in a natural manner in the non-dimensionalisation process of the governing equation (1), in the sense that the heat transfer/conduction dimensional group $\alpha/(\lambda_f\delta_f)$ in Eq. (1) has the dimension m^{-2}. Hence the dimensionless length variables, X_j, are obtained by multiplying the length variables x_j by $\sqrt{\alpha/(\lambda_f\delta_f)}$. In order to obtain dimensionless variables for the problem, the aspect ratios for the fin geometry, x_j/δ_f, are used which then results in the dimensionless parameter $\sqrt{\lambda_f/(\alpha\delta_f)}$, the so called maximum fin effectiveness for a planar rectangular fin, see Heggs [5], and for a radial rectangular fin, Heggs and Ooi [16]. It is interesting to note that the maximum fin effectiveness equation is equivalent to the reciprocal of the square root of the transverse Biot number, that is $Bi^{-1/2}$. Furthermore, it should be noted that the governing non-dimensionalised equation (5) is a Helmholtz-type equation, namely the modified Helmholtz equation. Although the boundary value problem given by Eqs. (5)–(7) is a direct, mixed, well-posed problem, its closed form analytical solution is not available even if the outer boundary is a circle, i.e. $\widetilde{\Gamma}_o=\{\underline{X}=(X_1,X_2)\mid X_1^2+X_2^2=R_o^2\}$. Hence a numerical method to solve the boundary value problem (5)–(7) must be employed.

3. Fin performance indicators

In this section, the performance indicators of the fins are briefly reviewed in the framework of the two-dimensional analysis. In the steady state, the *heat flow through the fin*, $\dot{Q}_f$, is obtained from the temperature profile either by considering the heat flow through the base of the fins or by integrating the heat flow from the domain occupied by the fin, see [2–5,15], namely

$$\dot{Q}_f^{(1)}=-\lambda_f(2\delta_f)\int_{\Gamma_{i1}\cup\Gamma_{i2}}\frac{\partial T_f(\underline{x})}{\partial v}\,dS(\underline{x})=-\lambda_f(2\delta_f)(T_b^1-T_\infty)\int_{\widetilde{\Gamma}_{i1}\cup\widetilde{\Gamma}_{i2}}\frac{\partial\theta_f(\underline{X})}{\partial\tilde{v}}\,dS(\underline{X}), \tag{14}$$

or

$$\dot{Q}_f^{(2)}=2\alpha\int\int_\Omega(T_f(\underline{x})-T_\infty)d\underline{x}=\lambda_f(2\delta_f)(T_b^1-T_\infty)\int\int_{\widetilde{\Omega}}\theta_f(\underline{X})d\underline{X}. \tag{15}$$

The *maximum possible heat flow through the fin*, denoted by $\dot{Q}_{f,max}$, is obtained by either substituting the (dimensionless) temperature gradient into Eq. (14), or substituting the (dimensionless) temperature into Eq. (15), and taking the limit of the corresponding integrals as the (dimensionless) fin length $l^{(s)}=r_o^{(s)}-r_i(L^{(s)}=R_o^{(s)}-R_i)$ tends to infinity. Equations (14) and (15) both lead to the following expression:

$$\dot{Q}_{f,max}=4\pi r_i\sqrt{\alpha\lambda_f\delta_f}\left[(T_b^1-T_\infty)+(T_b^2-T_\infty)\right]\frac{K_1(r_i/(\delta_f\zeta_{max}))}{K_0(r_i/(\delta_f\zeta_{max}))}. \tag{16}$$

This is equivalent to two independent tubes with polygonal fins of infinite dimensions attached to them. The maximum heat flow for each fin is identical to that found by Marin et al. [1] for the single polygonal fin. This is identical to the maximum heat flow that would occur for a one-dimensional radial rectangular fin, see Heggs and Ooi [16]. The ratio of the modified Bessel functions of the second kind of orders one and zero in Eq. (16) is plotted against the common arguments in Fig. 4. If the

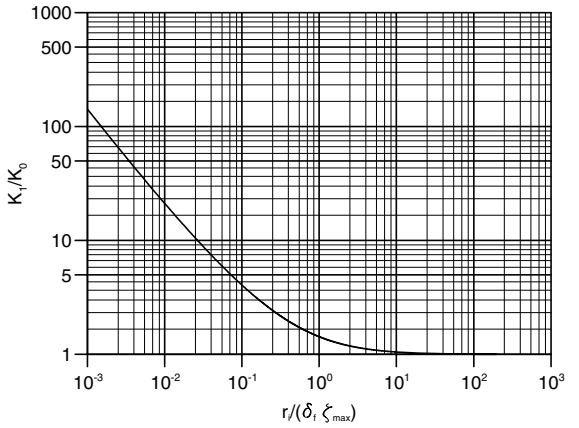

Fig. 4. The ratio between the modified Bessel functions K_1 and K_0 as a function of the non-dimensional parameter $r_i/(\delta_f\zeta_{max})$.

argument is greater than about 10 then the ratio can be taken to be unity. However, for small values of the argument, the value of the ratio quickly becomes quite large, such that for an argument value of 1.0×10^{-3}, the ratio is approximately 150.

The heat flow from the polygonal fins is bounded as follows:

$$\dot{Q}_{f,l^{(s)}\to(\sqrt{2}-1)r_i} < \dot{Q}_f < \dot{Q}_{f,max}. \tag{17}$$

The lower bound occurs as the fin length $l^{(s)} \to (\sqrt{2}-1)r_i$, or $r_o^{(s)} \to \sqrt{2}r_i$. Here the polygonal fin is a square of side $2r_i = \sqrt{2}r_o^{(s)}$ and the tubes touch the square at the midpoints of each side. The adiabatic boundary conditions imposed at the tip of the fin, see Eq. (3), will ensure that the solution does have a singularity where the two tubes coincide for this limiting condition. It should be mentioned that in Marin et al. [1] it was shown that the heat flow from a single isolated polygonal fin in this limiting case is approximated with an error of $O(10^{-4})$ by the one corresponding to a radial rectangular fin in the framework of the one-dimensional theory.

A *fin performance ratio*, PR, for these polygonal fins with two tubes passing through them can be defined in an identical manner to that recently proposed for isolated fins, see e.g. [1,5,6,16], namely

$$PR = \frac{\dot{Q}_f}{\dot{Q}_{f,max}}. \tag{18}$$

The fin performance ratio is bounded as follows:

$$\frac{\dot{Q}_{f,l^{(s)}\to(\sqrt{2}-1)r_i}}{\dot{Q}_{f,max}} < PR < 1. \tag{19}$$

Hence the introduction of the fin performance ratio provides an indicator which has an upper bound of unity, whilst the lower bound is dependent upon the ratio of the heat flow through the smallest sized polygonal fin ($r_o^{(s)} = \sqrt{2}r_i$) and the maximum possible heat flow.

The most commonly used fin performance indicator, the *fin efficiency*, η_f, see e.g. [2–4], is defined as the ratio of the heat flow through the fin to that which would flow if all the fin surface was at the base temperature. Unfortunately, if the two tubes have different temperatures then an expression for the fin efficiency cannot be obtained.

The fin performance indicator, the *fin effectiveness*, ζ_f, see e.g. [15,16], can be defined for the polygonal fins with two tubes passing through them. The definition is the ratio of the heat flow through the fin, $\dot{Q}_f$, to that which would flow to the primary surface (base area of the fin) if the fin was not present, $\dot{Q}$, where

$$\dot{Q} = 4\pi r_i\delta_f\alpha\left[\left(T_b^1 - T_\infty\right) + \left(T_b^2 - T_\infty\right)\right]. \tag{20}$$

Thus the fin effectiveness is given by

$$\zeta_f = \frac{\dot{Q}_f}{\dot{Q}}, \tag{21}$$

and is bounded as follows:

$$1 < \zeta_f < \frac{\dot{Q}_{f,max}}{\dot{Q}}. \tag{22}$$

Unlike the fin performance ratio, the fin effectiveness must be greater than unity, whilst the upper bound is given by the ratio of Eqs. (16) and (20), namely

$$\frac{\dot{Q}_{f,max}}{\dot{Q}} = \sqrt{\frac{\lambda_f}{\alpha\delta_f}}\frac{K_1(r_i/(\delta_f\zeta_{max}))}{K_0(r_i/(\delta_f\zeta_{max}))} \equiv \zeta_{max}\frac{K_1(r_i/(\delta_f\zeta_{max}))}{K_0(r_i/(\delta_f\zeta_{max}))}. \tag{23}$$

It is worth mentioning that $K_1/K_0 \to 1$ as $r_i/(\delta_f\zeta_{max}) \to \infty$ and, therefore, the one-dimensional model represents a very good approximation to the governing partial differential equation (1) for the temperature distribution in the polygonal fin assemblies under investigation. From the physical point of view this means that more heat passes through short radial rectangular fins than through the equivalent rectangular fins. It is interesting to note that in Eq. (23), the maximum fin effectiveness, ζ_{max}, for an isolated planar rectangular fin appears along with the ratio of the Bessel functions K_1/K_0. This ζ_{max} was used in the two-dimensional non-dimensionalisation procedure, see Eq. (4). The fin performance ratio, PR, is related to the fin effectiveness, ζ_f, as follows:

$$PR = \zeta_f \Big/ \left(\zeta_{max}\frac{K_1(r_i/(\delta_f\zeta_{max}))}{K_0(r_i/(\delta_f\zeta_{max}))}\right). \tag{24}$$

The equivalent one-dimensional radial rectangular fin with isothermal ($T_f = T_b^1$) and adiabatic conditions at its base and tip, respectively, has the following expressions for the heat flow, the maximum heat flow and the fin performance ratio:

$$\dot{Q}_{\mathrm{f}} = 4\pi r_{\mathrm{i}}\sqrt{\alpha\lambda_{\mathrm{f}}\delta_{\mathrm{f}}}\left(T_{\mathrm{b}}^{1}-T_{\infty}\right) \times \frac{K_1\left(\frac{r_{\mathrm{i}}}{\delta_{\mathrm{f}}\zeta_{\max}}\right)I_1\left(\frac{r_{\mathrm{o}}^{(\mathrm{r})}}{\delta_{\mathrm{f}}\zeta_{\max}}\right)-I_1\left(\frac{r_{\mathrm{i}}}{\delta_{\mathrm{f}}\zeta_{\max}}\right)K_1\left(\frac{r_{\mathrm{o}}^{(\mathrm{r})}}{\delta_{\mathrm{f}}\zeta_{\max}}\right)}{K_0\left(\frac{r_{\mathrm{i}}}{\delta_{\mathrm{f}}\zeta_{\max}}\right)I_1\left(\frac{r_{\mathrm{o}}^{(\mathrm{r})}}{\delta_{\mathrm{f}}\zeta_{\max}}\right)+I_0\left(\frac{r_{\mathrm{i}}}{\delta_{\mathrm{f}}\zeta_{\max}}\right)K_1\left(\frac{r_{\mathrm{o}}^{(\mathrm{r})}}{\delta_{\mathrm{f}}\zeta_{\max}}\right)} = 4\pi R_{\mathrm{i}}\delta_{\mathrm{f}}\lambda_{\mathrm{f}}\left(T_{\mathrm{b}}^{1}-T_{\infty}\right)\frac{K_1(R_{\mathrm{i}})I_1(R_{\mathrm{o}}^{(\mathrm{r})})-I_1(R_{\mathrm{i}})K_1(R_{\mathrm{o}}^{(\mathrm{r})})}{K_0(R_{\mathrm{i}})I_1(R_{\mathrm{o}}^{(\mathrm{r})})+I_0(R_{\mathrm{i}})K_1(R_{\mathrm{o}}^{(\mathrm{r})})}, \tag{25}$$

$$\dot{Q}_{\mathrm{f,max}} = 4\pi r_{\mathrm{i}}\sqrt{\alpha\lambda_{\mathrm{f}}\delta_{\mathrm{f}}}\left(T_{\mathrm{b}}^{1}-T_{\infty}\right)\frac{K_1\left(\frac{r_{\mathrm{i}}}{\delta_{\mathrm{f}}\zeta_{\max}}\right)}{K_0\left(\frac{r_{\mathrm{i}}}{\delta_{\mathrm{f}}\zeta_{\max}}\right)} = 4\pi R_{\mathrm{i}}\delta_{\mathrm{f}}\lambda_{\mathrm{f}}\left(T_{\mathrm{b}}^{1}-T_{\infty}\right)\frac{K_1(R_{\mathrm{i}})}{K_0(R_{\mathrm{i}})}, \tag{26}$$

$$\mathrm{PR} = \frac{\dot{Q}_{\mathrm{f}}}{\dot{Q}_{\mathrm{f,max}}} = \left\{1-\frac{K_1(R_{\mathrm{o}}^{(\mathrm{r})})}{K_1(R_{\mathrm{i}})}\Big/\frac{I_1(R_{\mathrm{i}})}{I_1(R_{\mathrm{o}}^{(\mathrm{r})})}\right\}\Big/\left\{1+\frac{K_1(R_{\mathrm{o}}^{(\mathrm{r})})}{K_0(R_{\mathrm{i}})}\Big/\frac{I_1(R_{\mathrm{i}})}{I_0(R_{\mathrm{o}}^{(\mathrm{r})})}\right\}. \tag{27}$$

Here I_0 and I_1 are the modified Bessel functions of the first kind of orders zero and one, respectively, whilst K_0 and K_1 are the modified Bessel functions of the second kind of orders zero and one, respectively.

By an appropriate regrouping of the problem parameters involved in expression (27) for the fin performance ratio in the one-dimensional theory, it can be seen that this performance indicator is a function of the ratio, $r_{\mathrm{i}}/\delta_{\mathrm{f}}$, of the inner radius and the half-thickness of the fin, the reduced fin length, $l/\delta_{\mathrm{f}} = (r_{\mathrm{o}}^{(\mathrm{r})}-r_{\mathrm{i}})/\delta_{\mathrm{f}}$, and the maximum fin effectiveness, $\zeta_{\max}$, i.e. $\mathrm{PR} = \mathrm{PR}(r_{\mathrm{i}}/\delta_{\mathrm{f}}, l/\delta_{\mathrm{f}}, \zeta_{\max})$. Since the first two parameters of the problem ($r_{\mathrm{i}}/\delta_{\mathrm{f}}$, l/δ_{f}) contain information on the geometry of the fin and the last one ($\zeta_{\max}$) directly reflects the physics of the heat flow through the fin, the fin performance ratio is expected to be a comprehensive performance indicator of the fin under consideration in both one- and two-dimensional theories. On combining expressions (25)–(27) we obtain the following expression for the heat flow through the fin, see also Marin et al. [1],

$$\dot{Q}_{\mathrm{f}} = 4\pi r_{\mathrm{i}}\delta_{\mathrm{f}}\alpha\mathrm{PR}(r_{\mathrm{i}}/\delta_{\mathrm{f}}, l/\delta_{\mathrm{f}}, \zeta_{\max})\left(T_{\mathrm{b}}^{1}-T_{\infty}\right) \times \frac{K_1(r_{\mathrm{i}}/(\delta_{\mathrm{f}}\zeta_{\max}))}{K_0(r_{\mathrm{i}}/(\delta_{\mathrm{f}}\zeta_{\max}))}. \tag{28}$$

Consequently, it would be convenient if the two-dimensional heat flow could be predicted within an acceptable tolerance by using the one-dimensional theory. Then, the heat flow, $\dot{Q}_{\mathrm{f}}$, and the maximum possible heat flow, $\dot{Q}_{\mathrm{f,max}}$, corresponding to the polygonal fin assembly under investigation, respectively, could be predicted by

$$\dot{Q}_{\mathrm{f}} = 4\pi r_{\mathrm{i}}\sqrt{\alpha\lambda_{\mathrm{f}}\delta_{\mathrm{f}}}\sum_{j=1}^{2}\left(T_{\mathrm{b}}^{j}-T_{\infty}\right) \times \frac{K_1\left(\frac{r_{\mathrm{i}}}{\delta_{\mathrm{f}}\zeta_{\max}}\right)I_1\left(\frac{r_{\mathrm{o}}^{(\mathrm{r})}}{\delta_{\mathrm{f}}\zeta_{\max}}\right)-I_1\left(\frac{r_{\mathrm{i}}}{\delta_{\mathrm{f}}\zeta_{\max}}\right)K_1\left(\frac{r_{\mathrm{o}}^{(\mathrm{r})}}{\delta_{\mathrm{f}}\zeta_{\max}}\right)}{K_0\left(\frac{r_{\mathrm{i}}}{\delta_{\mathrm{f}}\zeta_{\max}}\right)I_1\left(\frac{r_{\mathrm{o}}^{(\mathrm{r})}}{\delta_{\mathrm{f}}\zeta_{\max}}\right)+I_0\left(\frac{r_{\mathrm{i}}}{\delta_{\mathrm{f}}\zeta_{\max}}\right)K_1\left(\frac{r_{\mathrm{o}}^{(\mathrm{r})}}{\delta_{\mathrm{f}}\zeta_{\max}}\right)} = 4\pi R_{\mathrm{i}}\delta_{\mathrm{f}}\lambda_{\mathrm{f}}\sum_{j=1}^{2}\left(T_{\mathrm{b}}^{j}-T_{\infty}\right) \times \frac{K_1(R_{\mathrm{i}})I_1(R_{\mathrm{o}}^{(\mathrm{r})})-I_1(R_{\mathrm{i}})K_1(R_{\mathrm{o}}^{(\mathrm{r})})}{K_0(R_{\mathrm{i}})I_1(R_{\mathrm{o}}^{(\mathrm{r})})+I_0(R_{\mathrm{i}})K_1(R_{\mathrm{o}}^{(\mathrm{r})})}, \tag{29}$$

$$\dot{Q}_{\mathrm{f,max}} = 4\pi r_{\mathrm{i}}\sqrt{\alpha\lambda_{\mathrm{f}}\delta_{\mathrm{f}}}\sum_{j=1}^{2}\left(T_{\mathrm{b}}^{j}-T_{\infty}\right)\frac{K_1\left(\frac{r_{\mathrm{i}}}{\delta_{\mathrm{f}}\zeta_{\max}}\right)}{K_0\left(\frac{r_{\mathrm{i}}}{\delta_{\mathrm{f}}\zeta_{\max}}\right)} = 4\pi R_{\mathrm{i}}\delta_{\mathrm{f}}\lambda_{\mathrm{f}}\sum_{j=1}^{2}\left(T_{\mathrm{b}}^{j}-T_{\infty}\right)\frac{K_1(R_{\mathrm{i}})}{K_0(R_{\mathrm{i}})}, \tag{30}$$

Moreover, from Eqs. (27), (29) and (30) we obtain the following expression for the heat flow through the polygonal fin assembly

$$\dot{Q}_{\mathrm{f}} = 4\pi r_{\mathrm{i}}\delta_{\mathrm{f}}\alpha\mathrm{PR}(r_{\mathrm{i}}/\delta_{\mathrm{f}}, l/\delta_{\mathrm{f}}, \zeta_{\max}) \times \sum\nolimits_{j=1}^{2}\left(T_{\mathrm{b}}^{j}-T_{\infty}\right)\frac{K_1(r_{\mathrm{i}}/(\delta_{\mathrm{f}}\zeta_{\max}))}{K_0(r_{\mathrm{i}}/(\delta_{\mathrm{f}}\zeta_{\max}))}. \tag{31}$$

The above expression would be of considerable practical importance for determining the value of the heat flow, $\dot{Q}_{\mathrm{f}}$, through a polygonal fin assembly characterised by the coefficient of convective heat transfer, α, the thermal conductivity, λ_{f}, the half-thickness, δ_{f}, the inner radius, r_{i}, and the fin length, $l^{(\mathrm{s})} = r_{\mathrm{o}}^{(\mathrm{s})} - r_{\mathrm{i}}$, by using the design charts for the prediction of the performance ratio, PR, of equivalent radial rectangular fins, i.e. radial rectangular fins characterised by the same coefficient of convective heat transfer, thermal conductivity, half-fin thickness and inner radius and the fin length $l = r_{\mathrm{o}}^{(\mathrm{r})} - r_{\mathrm{i}}$, such that $r_{\mathrm{o}}^{(\mathrm{r})} = \sqrt{2/\pi}r_{\mathrm{o}}^{(\mathrm{s})}$, see Fig. 5, and the graph of the function K_1/K_0, see Fig. 4. Furthermore, the charts for the prediction of the fin performance ratio give very good information on the fin performance, the geometry (dimensions) of the fin and the fin material. More specifically, from Fig. 5 it can be seen that such a design chart consists of three specific regions. The first one which is located above the graph of the function PR = 0.99, say, corresponds to very long fins, i.e. too much material has been used for the fin. The region below the graph of the function PR = 0.01, say, characterises fins made of materials having properties unsuitable for design purposes. Finally, the region between the graphs of the functions PR = 0.01 and PR = 0.99 is of practical importance and gives the designers comprehensive information on both the geometry of the fin and the physics of the heat flow through the fin. It should be

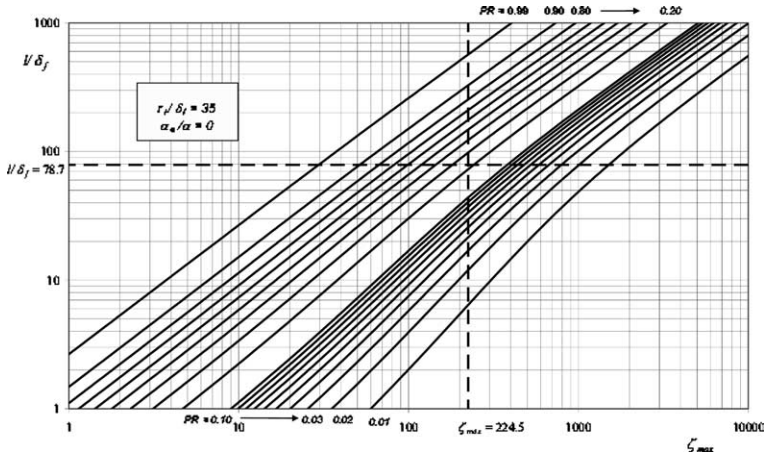

Fig. 5. Design chart for the prediction of the performance ratio PR of radial rectangular fins with $r_i = 7.0 \times 10^{-3}$ m and $\delta_f = 0.2 \times 10^{-3}$ m.

mentioned that the normal practice is to use a fin efficiency with a value greater than 0.80 and this will correspond to a fin performance ratio with a value of around 0.40 or less. Consequently, the fin performance ratio, PR, is a better fin performance indicator than the fin efficiency, η_f.

4. The boundary element method

The governing non-dimensionalised partial differential equation (5) can also be formulated in integral form, see e.g. Chen and Zhou [17], as follows:

$$c(\underline{X})\theta_f(\underline{X}) + \int_{\partial\widetilde{\Omega}} \frac{\partial E(\underline{X},\underline{Y})}{\partial \widetilde{\nu}} \theta_f(\underline{Y})\, dS(\underline{Y}) = \int_{\partial\widetilde{\Omega}} E(\underline{X},\underline{Y}) \frac{\partial \theta_f(\underline{Y})}{\partial \widetilde{\nu}}\, dS(\underline{Y}) \tag{32}$$

for $\underline{X} \in \widetilde{\Omega} \cup \partial\widetilde{\Omega}$, where $c(\underline{X}) = 1$ for $\underline{X} \in \widetilde{\Omega}$ and $c(\underline{X}) = 1/2$ for $\underline{X} \in \partial\widetilde{\Omega}$ (smooth), and E is the fundamental solution for the modified Helmholtz equation (5), which is given by

$$E(\underline{X},\underline{Y}) = \frac{1}{2\pi} K_0(r(\underline{X},\underline{Y})). \tag{33}$$

Here $r(\underline{X},\underline{Y})$ represents the distance between the load point $\underline{X}$ and the field point $\underline{Y}$. Alternatively, one can also use the real part of the complex fundamental solution E for the modified Helmholtz equation in the boundary integral equation (32), namely

$$E(\underline{X},\underline{Y}) = \mathrm{Re}\left\{ \frac{i}{4} H_0^{(1)}(ir(\underline{X},\underline{Y})) \right\}, \tag{34}$$

where $i = \sqrt{-1}$ and $H_0^{(1)}$ is the Hankel function of the first kind of order zero.

It should be noted that in practice the boundary integral equation (32) can rarely be solved analytically and thus a numerical approximation is required. A BEM with piecewise constant boundary elements is used in order to solve the direct, mixed, well-posed boundary value problem (5)–(7). Consequently, the outer boundary $\widetilde{\Gamma}_o$ is approximated by N_o straight line segments in a counterclockwise sense and the inner boundaries $\widetilde{\Gamma}_{i1}$ and $\widetilde{\Gamma}_{i2}$ are approximated by N_{i1} and N_{i2} straight line segments, respectively, in a clockwise sense, such that the boundary $\partial\widetilde{\Omega}$ is discretised into $N = N_o + N_{i1} + N_{i2}$ boundary elements, whilst the non-dimensional temperature and the non-dimensional flux are considered to be constant and take their values at the midpoint, i.e. the collocation point, also known as the node, of each element. More specifically, we have

$$\begin{aligned}
&\widetilde{\Gamma}_o \approx \bigcup_{n=1}^{N_o} \widetilde{\Gamma}_o^{(n)}, \quad \widetilde{\Gamma}_o^{(n)} = \left[\underline{Y_o}^{n-1}, \underline{Y_o}^{n}\right], \quad n = 1,\ldots,N_o, \quad \underline{Y_o}^{N_o} = \underline{Y_o}^{0},\\
&\widetilde{\Gamma}_{i1} \approx \bigcup_{n=1}^{N_{i1}} \widetilde{\Gamma}_{i1}^{(n)}, \quad \widetilde{\Gamma}_{i1}^{(n)} = \left[\underline{Y_{i1}}^{n-1}, \underline{Y_{i1}}^{n}\right], \quad n = 1,\ldots,N_{i1}, \quad \underline{Y_{i1}}^{N_{i1}} = \underline{Y_{i1}}^{0},\\
&\widetilde{\Gamma}_{i2} \approx \bigcup_{n=1}^{N_{i2}} \widetilde{\Gamma}_{i2}^{(n)}, \quad \widetilde{\Gamma}_{i2}^{(n)} = \left[\underline{Y_{i2}}^{n-1}, \underline{Y_{i2}}^{n}\right], \quad n = 1,\ldots,N_{i2}, \quad \underline{Y_{i2}}^{N_2} = \underline{Y_{i2}}^{0},
\end{aligned} \tag{35}$$

where

$$\begin{aligned}
&\underline{X}^{n} = \left(\underline{Y_o}^{n-1} + \underline{Y_o}^{n}\right)/2, \quad n = 1,\ldots,N_o,\\
&\underline{X}^{N_o+n} = \left(\underline{Y_{i1}}^{n-1} + \underline{Y_{i1}}^{n}\right)/2, \quad n = 1,\ldots,N_{i1},\\
&\underline{X}^{N_o+N_{i1}+n} = \left(\underline{Y_{i2}}^{n-1} + \underline{Y_{i2}}^{n}\right)/2, \quad n = 1,\ldots,N_{i2},
\end{aligned} \tag{36}$$

and

$$\theta_f(\underline{Y}) = \theta_f(\underline{X}^n), \quad \frac{\partial\theta_f(\underline{Y})}{\partial\widetilde{v}} = \frac{\partial\theta_f(\underline{X}^n)}{\partial\widetilde{v}}, \quad \underline{Y} \in \widetilde{\Gamma}_n, \quad n = 1,\ldots,N, \tag{37}$$

where $\widetilde{\Gamma}_n = \widetilde{\Gamma}_o^{(n)}$ for $n = 1,\ldots,N_o$, $\widetilde{\Gamma}_{N_o+n} = \widetilde{\Gamma}_{i1}^{(n)}$ for $n = 1,\ldots,N_{i1}$ and $\widetilde{\Gamma}_{N_o+N_{i1}+n} = \widetilde{\Gamma}_{i2}^{(n)}$ for $n = 1,\ldots,N_{i2}$.

By applying the boundary integral equation (32) at each collocation point $\underline{X}^m$, $m = 1,\ldots,N$, and taking into account the fact that the boundary is always smooth at these points, we arrive at the following system of linear algebraic equations

$$\boldsymbol{A\theta} = \boldsymbol{B\varphi}, \tag{38}$$

where the matrices $\boldsymbol{A},\boldsymbol{B} \in \mathbb{R}^{N\times N}$ depend solely on the geometry of the boundary $\partial\widetilde{\Omega}$ and the vectors $\boldsymbol{\theta},\boldsymbol{\varphi} \in \mathbb{R}^N$ consist of the discretised values of the non-dimensional temperature and flux on the boundary $\partial\widetilde{\Omega}$, namely

$$\theta_m = \theta_f(\underline{X}^m), \quad \varphi_m = \frac{\partial\theta_f(\underline{X}^m)}{\partial\widetilde{v}}, \quad m = 1,\ldots,N, \tag{39}$$

$$A_{nm} = \frac{1}{2}\delta_{nm} + A_n(\underline{X}^m) = \frac{1}{2}\delta_{nm} + \int_{\widetilde{\Gamma}_n} \frac{\partial E(\underline{X}^m,\underline{Y})}{\partial\widetilde{v}}\,\mathrm{d}S(\underline{Y}), \quad m,n = 1,\ldots,N, \tag{40}$$

$$B_{nm} = B_n(\underline{X}^m) = \int_{\widetilde{\Gamma}_n} E(\underline{X}^m,\underline{Y})\,\mathrm{d}S(\underline{Y}), \quad m,n = 1,\ldots,N, \tag{41}$$

where δ_{nm} is the Kronecker tensor. It should be noted that Eq. (38) represents a system of N linear algebraic equations with $2N$ unknowns. The discretisation of the boundary conditions (6) and (7) provides the values of N of the unknowns and the problem reduces to solving a system of N equations with N unknowns which can be generically written as follows:

$$\boldsymbol{Cx} = \boldsymbol{f}, \tag{42}$$

where the right-hand side vector $\boldsymbol{f} \in \mathbb{R}^N$ is computed using the boundary conditions (6) and (7), the system matrix $\boldsymbol{C} \in \mathbb{R}^{N\times N}$ depends solely on the geometry of the boundary $\partial\widetilde{\Omega}$ and the vector $\boldsymbol{x} \in \mathbb{R}^N$ contains the unknown values of the non-dimensional temperature on the outer boundary $\widetilde{\Gamma}_o$ and the non-dimensional flux on the inner boundaries $\widetilde{\Gamma}_{i1}$ and $\widetilde{\Gamma}_{i2}$.

Once the unknown values of the non-dimensional temperature and flux on the outer and inner boundaries, respectively, have been computed then by employing the discretisation of the boundary integral equation (32) for internal points $\underline{X} \in \widetilde{\Omega}$, the BEM approximation of the non-dimensional temperature θ_f can be obtained at any internal point in the form

$$\theta_f(\underline{X}) = \sum_{n=1}^{N} \{B_n(\underline{X})\varphi_n - A_n(\underline{X})\theta_n\}, \tag{43}$$

where $A_n(\underline{X})$ and $B_n(\underline{X})$ are given by relations (40) and (41), respectively, with $\underline{X}^m = \underline{X}$.

5. Numerical results

The numerical analysis presented in this section for the square fin assembly is based on typical geometries and operating conditions used in evaporators and condensers in commercial refrigeration storage units, see e.g. Rizvi [18]. We illustrate the numerical results obtained using the BEM described in the previous section by investigating the convergence, stability and consistency of the numerical method proposed. In addition, the performance of the square fin assembly is studied in the two-dimensional approach by comparing the performance ratio and the heat flow through the square fin assembly corresponding to the expressions (14) and (15), respectively, with their values obtained by considering the one-dimensional theory for two radial fins equivalent with each of the two square fins which compose the fin assembly under investigation, see Eqs. (27) and (31). To do so, we consider polygonal fins on a square pitch characterised by the inner radius (outer radius of the tube) $r_i = 7.0\times10^{-3}$ m, the radius of the circle which encloses a single square fin $r_o^{(s)} = 28.49\times10^{-3}$m, the half-fin thicknesses $\delta_f = 0.1\times10^{-3}$ m and $\delta_f = 0.2\times10^{-3}$ m and the thermal conductivity $\lambda_f = 202.4$ W m^{-1} K^{-1}, as well as the equivalent radial fin $r_o^{(r)} = 22.74\times10^{-3}$m. In the sequel, the fin length is given by $l = r_o^{(r)} - r_i$, where $r_o^{(r)}$ is the outer radius of the equivalent radial rectangular fin, the convective heat transfer coefficient is given by $\alpha = 20.0$ W m^{-2} K^{-1}, $T_b^1 - T_\infty = 1$ K and $(T_b^2 - T_\infty)/(T_b^1 - T_\infty) \in \{0.10, 0.50, 0.90\}$ in order to illustrate the different temperatures of the tubes.

The solution to the boundary value problem (5)–(7) by any technique which involves approximations in the solution procedure invariably includes an error. In the case of the BEM, the errors in the numerical solutions are related to the associated mesh size, they diminish as the mesh size discretisation is refined and, consequently, the approximate solutions approach the exact solution. Three levels of discretisation which are given by the number of boundary elements used to discretise the square fin assembly under investigation, namely $N \in \{100, 200, 400\}$, $N_{i1} = N_{i2} = N_o/3 = N/5$, are used in order to check for the convergence of the proposed BEM.

Fig. 6(a)–(c) represent the numerical non-dimensional temperature distribution θ_f in the square fin assembly with $\delta_f = 0.1\times10^{-3}$ m ($l/\delta_f = 157.34$ and $\zeta_{max} = 318.11$) and $(T_b^2 - T_\infty)/(T_b^1 - T_\infty) \in \{0.10, 0.50, 0.90\}$, obtained with $N = 400$ boundary elements. From the tube on the left in Fig. 6(a) it can be seen that if $(T_b^2 - T_\infty)/(T_b^1 - T_\infty) = 0.10$ then heat not only flows from the hotter tube to the air, but also to the colder

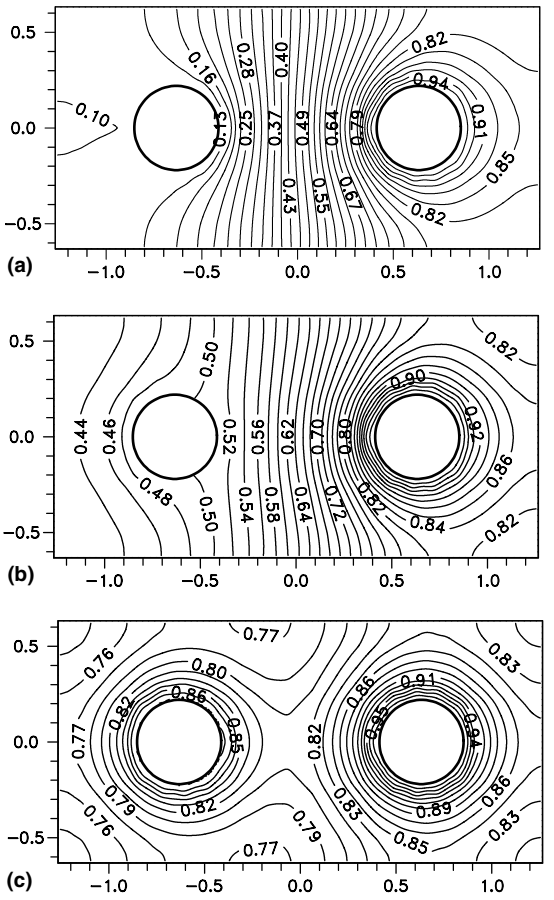

Fig. 6. The non-dimensional temperature distribution, θ_f, in the square fin assembly obtained using $N = 400$ boundary elements, $\alpha = 20.0\ \mathrm{W\,m^{-2}\,K^{-1}}$, $\delta_f = 0.1 \times 10^{-3}$ m, $r_i = 7.0 \times 10^{-3}$ m, $r_o^{(s)} = 28.49 \times 10^{-3}$ m, $\lambda_f = 202.4\ \mathrm{W\,m^{-1}\,K^{-1}}$, i.e. $l/\delta_f = 157.34$ and $\zeta_{max} = 318.11$, (a) $(T_b^2 - T_\infty)/(T_b^1 - T_\infty) = 0.10$, (b) $(T_b^2 - T_\infty)/(T_b^1 - T_\infty) = 0.50$ and (c) $(T_b^2 - T_\infty)/(T_b^1 - T_\infty) = 0.90$.

tube. The temperature of the fin around the colder tube is completely above the temperature of the tube. Hence the polygonal fin assembly for this condition has provided a conductive path between the two tubes even though there is a finite temperature difference between the tubes, the fin surface and the surrounding air. A similar effect is observed from Fig. 6(b), but it is much less severe and only a small portion of the fin surface around the tube on the left is above the tube temperature. However, if the temperature difference between the tubes is low, Fig. 6(c), i.e. $(T_b^2 - T_\infty)/(T_b^1 - T_\infty) = 0.90$, then the heat solely flows into the air. Similar results have been obtained for square fin assemblies with $\delta_f = 0.2 \times 10^{-3}$ m and therefore they are not presented here. Although an analytical solution is not available for the examples under investigation, it is reported that the BEM solutions for the non-dimensional temperature display a convergent behaviour as the corresponding discretisation is refined. Furthermore, from Fig. 6 it can be seen that the non-dimensional temperature profiles in the square fin assembly are indeed two-dimensional for different values of the ratio between the temperatures of the tubes, and hence we can conclude that the two-dimensional treatment of the square fin assemblies is fully justified. In addition, since the boundary conditions (6) and (7) contain the analytical values of the non-dimensional temperature on the inner boundaries $\widetilde{\Gamma}_{i1}$ and $\widetilde{\Gamma}_{i2}$, and the flux on the outer boundary $\widetilde{\Gamma}_o$, respectively, then these boundary data are polluted with numerical noise and therefore the numerical method proposed is also stable.

In the context of numerical methods, such as finite-difference, finite element and boundary element methods, the integrations from relations (14) and (15) can be performed employing an appropriate quadrature formula. However, as these numerical techniques only provide approximate solutions, the corresponding values for the integrations in Eqs. (14) and (15) need not be exactly the same, although, these should agree to within an acceptable tolerance in order for the numerical solutions to be satisfactory. Therefore, in the subsequent calculations $\dot{Q}_f^{(1)}$ and $\dot{Q}_f^{(2)}$ denote the values of the heat flow through the square fin assembly corresponding to the expressions (14) and (15), respectively. It is important to mention that a further requirement for the numerical solutions to be satisfactory is that the corresponding heat flows through the square fin assembly under investigation show a convergent behaviour as the order of the approximation is improved.

In Table 1 we present the values of the heat flows $\dot{Q}_f^{(1)}$ and $\dot{Q}_f^{(2)}$ given by Eqs. (14) and (15), respectively, as well as the performance ratio PR, see Eq. (18), obtained for square fin assemblies with $\delta_f = 0.1 \times 10^{-3}$ m ($l/\delta_f = 157.34$ and $\zeta_{max} = 318.11$), $\delta_f = 0.2 \times 10^{-3}$ m ($l/\delta_f = 78.70$ and $\zeta_{max} = 224.50$), $(T_b^2 - T_\infty)/(T_b^1 - T_\infty) \in \{0.10, 0.50, 0.90\}$ and using the two-dimensional BEM proposed in this study. For comparison, the analytical values for the equivalent radial fin given by the one-dimensional theory, i.e. expressions (25) and (27), are also listed in Table 1. It can be seen from this table that all the aforementioned fin performance indicators exhibit convergence with respect to the mesh refinement and the numerical results obtained for the heat flow through the square fin assembly and the performance ratio are very good approximations for their analytical values of the equivalent radial rectangular fin. The numerical technique proposed is also consistent, in the sense that the difference between the computed heat flows $\dot{Q}_f^{(1)}$ and $\dot{Q}_f^{(2)}$ is $O(10^{-4})$ for all the thicknesses, ratios between the temperatures of the tubes and discretisations considered. Moreover, as further refinement of the boundary discretisation is impractical, the limiting

Table 1
The 1D analytical, the 2D BEM and the corresponding Richardson's extrapolation values for the heat flows $\dot{Q}_f^{(1)}$ and $\dot{Q}_f^{(2)}$ and the performance ratio PR for the square fin assembly and the equivalent radial fin, obtained with $\delta_f = 0.1 \times 10^{-3}$ m ($l/\delta_f = 157.34$ and $\zeta_{max} = 318.11$), $\delta_f = 0.2 \times 10^{-3}$ m ($l/\delta_f = 78.70$ and $\zeta_{max} = 224.50$) and $(T_b^2 - T_\infty)/(T_b^1 - T_\infty) \in \{0.10, 0.50, 0.90\}$

δ_f [m]	$\frac{T_b^2 - T_\infty}{T_b^1 - T_\infty}$	Fin type	Solution type	$\dot{Q}_f^{(1)}$	$\dot{Q}_f^{(2)}$	PR
0.1×10^{-3}	0.10	Radial (1D)	Analytical	0.05649	0.05649	0.35394
		Square (2D)	$N = 100$	0.05634	0.05644	0.35297
			$N = 200$	0.05634	0.05652	0.35300
			$N = 400$	0.05634	0.05654	0.35301
			Richardson's extrapolation	0.05634	0.05655	0.35302
	0.50	Radial (1D)	Analytical	0.07703	0.07703	0.35394
		Square (2D)	$N = 100$	0.07682	0.07696	0.35297
			$N = 200$	0.07683	0.07707	0.35300
			$N = 400$	0.07683	0.07710	0.35301
			Richardson's extrapolation	0.07683	0.07711	0.35302
	0.90	Radial (1D)	Analytical	0.09758	0.09758	0.35394
		Square (2D)	$N = 100$	0.09731	0.09748	0.35297
			$N = 200$	0.09731	0.09763	0.35300
			$N = 400$	0.09732	0.09766	0.35301
			Richardson's extrapolation	0.09731	0.09767	0.35302
0.2×10^{-3}	0.10	Radial (1D)	Analytical	0.06028	0.06028	0.22152
		Square (2D)	$N = 100$	0.06023	0.06024	0.22135
			$N = 200$	0.06020	0.06029	0.22123
			$N = 400$	0.06019	0.06030	0.22121
			Richardson's extrapolation	0.06019	0.06030	0.22121
	0.50	Radial (1D)	Analytical	0.08220	0.08220	0.22152
		Square (2D)	$N = 100$	0.08213	0.08214	0.22135
			$N = 200$	0.08209	0.08221	0.22123
			$N = 400$	0.08208	0.08223	0.22121
			Richardson's extrapolation	0.08208	0.08224	0.22121
	0.90	Radial (1D)	Analytical	0.10412	0.10412	0.22152
		Square (2D)	$N = 100$	0.10404	0.10405	0.22135
			$N = 200$	0.10398	0.10413	0.22123
			$N = 400$	0.10397	0.10415	0.22121
			Richardson's extrapolation	0.10397	0.10416	0.22121

values of $\dot{Q}_f^{(1)}$, $\dot{Q}_f^{(2)}$ and PR corresponding to the square fin assemblies investigated in this study are computed by the extrapolation of their BEM solutions obtained for $N \in \{100, 200, 400\}$ and by employing Richardson's formula [19]. These values are very good approximations for the heat flow, as well as for the performance ratio, in all the cases analysed in this paper. However, it is reported that the numerical results obtained for the fin performance indicators in the case of square fin assemblies are less accurate than their numerical values retrieved for a single polygonal fin on square pitches, see [1].

It is interesting to note that the presence of conductive paths between the tubes observed in Fig. 6(a) and (b) for $(T_b^2 - T_\infty)/(T_b^1 - T_\infty) \in \{0.10, 0.50\}$ does not affect the heat transferred from the tubes and fins to the air, when predicted by the one-dimensional theory. The values of the fin performance ratios for the two-dimensional numerical results and the one-dimensional theory are virtually identical, irrespective of the temperatures of the two tubes. In the one-dimensional theory postulation, Eq. (31), the two tubes are taken to be independent of each other. Therefore, for conditions where the conductive paths occur more heat is extracted from the hotter tube to compensate for the heat flow into the colder tube, but at the same time ensuring that the heat flow to the surrounding air is equivalent to that from the individual tubes and the polygonal fin assembly. This has been verified by evaluating the heat flow from each tube from the two-dimensional numerical results using Eq. (14), but only for the individual tubes, such that

$$\dot{Q}^{(1)}_{f,h} + \dot{Q}^{(1)}_{f,c} = \dot{Q}^{(1)}_{f}, \tag{44}$$

where $\dot{Q}^{(1)}_{f,h}$ and $\dot{Q}^{(1)}_{f,c}$ are the heat flows from the hotter (tube 1) and the colder (tube 2) tubes, respectively. These values are tabulated in Table 2 for all the cases detailed in Table 1. These remarkable results have not been reported before for polygonal fin assemblies.

The linearity of the mathematical representation of this polygonal fin assembly with two tubes passing through the fin, and the imposition of adiabatic boundary condition on the edges of the fin, Eq. (7), are responsible. Identical results for the heat flow will be obtained if the problem is considered as a single square fin with one tube passing through it, but the tube temperature in this case is the summation of the two individual tubes, i.e. $\theta^1 + \theta^2$. This phenomenon is analogous to the detrimental transverse conduction paths found in plate-fin heat exchangers, where the fin surfaces are attached at each end to the parting sheets of each fluid channel. This is the so-called half-fin length assumption, see Prasad [20] and Geraldelli [21].

6. Investigation of the range of applicability of the use of the one-dimensional analytical performance ratio for a polygonal fin with two tubes on a square pitch

The results reported in Tables 1 and 2 are for two polygonal fins with different thicknesses, $\delta_f = 0.1 \times 10^{-3}$ m and $\delta_f = 0.2 \times 10^{-3}$ m, respectively. The other dimensions and values of the heat transfer coefficient and thermal conductivity are the same in both cases. For the thicker fin, there are conductive paths between the tubes for a wider range of the temperature differences between the two tubes than were obtained for the thinner fin. The parameters for the second case are $r_i/\delta_f = 35$, $l/\delta_f = 78.70$ and $\zeta_{max} = 224.50$, and the one-dimensional value of the PR for the equivalent radial rectangular fin was 0.22152. This is illustrated in Fig. 5 by the intersection of the dashed vertical and horizontal lines corresponding to $\zeta_{max} = 224.50$ and $l/\delta_f = 78.70$, respectively.

In order to provide more confidence in the use of the one-dimensional performance ratio of the equivalent radial rectangular fin for the prediction of the heat flow

Table 2
The 2D BEM and the corresponding Richardson's extrapolation values for the heat flows $\dot{Q}^{(1)}_{f}$, $\dot{Q}^{(1)}_{f,h}$ and $\dot{Q}^{(1)}_{f,c}$ obtained for the square fin assembly with $\delta_f = 0.1 \times 10^{-3}$ m ($l/\delta_f = 157.34$ and $\zeta_{max} = 318.11$), $\delta_f = 0.2 \times 10^{-3}$ m ($l/\delta_f = 78.70$ and $\zeta_{max} = 224.50$) and $(T^2_b - T_\infty)/(T^1_b - T_\infty) \in \{0.10, 0.50, 0.90\}$

δ_f [m]	$\frac{T^2_b - T_\infty}{T^1_b - T_\infty}$	Solution type	$\dot{Q}^{(1)}_{f}$	$\dot{Q}^{(1)}_{f,h}$	$\dot{Q}^{(1)}_{f,c}$
0.1×10^{-3}	0.10	$N = 100$	0.05634	0.08308	−0.02671
		$N = 200$	0.05634	0.08324	−0.02690
		$N = 400$	0.05634	0.08328	−0.02695
		Richardson's extrapolation	0.05634	0.08329	−0.02697
	0.50	$N = 100$	0.07682	0.06890	0.00792
		$N = 200$	0.07683	0.06901	0.00783
		$N = 400$	0.07683	0.06903	0.00781
		Richardson's extrapolation	0.07683	0.06903	0.00781
	0.90	$N = 100$	0.09731	0.05475	0.04256
		$N = 200$	0.09731	0.05478	0.04254
		$N = 400$	0.09732	0.05478	0.04253
		Richardson's extrapolation	0.09731	0.05478	0.04252
0.2×10^{-3}	0.10	$N = 100$	0.06023	0.12676	−0.06653
		$N = 200$	0.06020	0.12708	−0.06688
		$N = 400$	0.06019	0.12716	−0.06697
		Richardson's extrapolation	0.06019	0.12719	−0.06700
	0.50	$N = 100$	0.08213	0.09476	−0.01263
		$N = 200$	0.08209	0.09492	−0.01283
		$N = 400$	0.08208	0.09497	−0.01289
		Richardson's extrapolation	0.08208	0.09499	−0.01291
	0.90	$N = 100$	0.10404	0.06276	0.04128
		$N = 200$	0.10398	0.06277	0.04121
		$N = 400$	0.10397	0.06277	0.04120
		Richardson's extrapolation	0.10397	0.06277	0.04120

from the polygonal fins with two tubes on a square pitch, we have investigated the relative percentage error between the one- and two-dimensional predictions over a wide range of values of the performance ratio. The value of the temperature differences between the two tubes $(T_b^2 - T_\infty)/(T_b^1 - T_\infty)$ has been fixed at 0.90 and the PR range investigated is from 0.99 down to 0.01. Two sets of calculations are reported here. In the first case, ζ_{max} is kept constant at 224.50 and the aspect ratio l/δ_f has been varied. This range can be seen by the dashed vertical line in Fig. 5 and is $l/\delta_f \in (7.5, 600)$. In the second set of calculations, the aspect ratio l/δ_f is kept constant at 78.70 and the maximum fin effectiveness ζ_{max} has been varied. This range is covered by the dashed horizontal line in Fig. 5 and is given by $\zeta_{max} \in (30, 1500)$.

The value of the performance ratio increases for larger values of the aspect ratio l/δ_f. For the geometry of this case, the two-dimensional model is only applicable provided that $l/\delta_f > (2/\sqrt{\pi} - 1)r_i/\delta_f$, that is when $r_o^{(s)}$ is greater than $\sqrt{2}r_i$. If $l/\delta_f \leqslant (2/\sqrt{\pi} - 1)r_i/\delta_f$ then the two-dimensional mathematical model no longer represents the geometry.

The values of the performance ratio, PR, obtained from the one-dimensional theory and the numerical solution of the two-dimensional model are plotted against the aspect ratio, l/δ_f, in Fig. 7(a). The one-dimensional theory appears to be an excellent approximation for the prediction of the performance ratio for the two-dimensional model. In order to get a better understanding of the qualitative behaviour of the above dependence, we define the relative percentage error, see also Marin et al. [1],

$$\mathrm{err}(\mathrm{PR}) = \frac{\mathrm{PR}^{(\mathrm{num})} - \mathrm{PR}^{(\mathrm{an})}}{\mathrm{PR}^{(\mathrm{an})}} \times 100, \tag{45}$$

where $\mathrm{PR}^{(\mathrm{an})}$ and $\mathrm{PR}^{(\mathrm{num})}$ are the analytical and the numerical values for the performance ratio, respectively. Fig. 7(b) illustrates the evolution of the error err(PR) given by expression (45) with respect to the reduced fin length, l/δ_f, obtained for the square fin assembly using various BEM discretisations. The error is very dependent upon the number of boundary elements, especially so for values of the aspect ratio l/δ_f less than about 100. However, for the largest number of boundary elements, $N = 400$, the error is always negative, but the value over the entire range of aspect ratios is within -0.5%. Hence the one-dimensional theory is an excellent prediction for the polygonal fin with two tubes on a square pitch for this fixed value of the maximum fin effectiveness, $\zeta_{max} = 224.50$.

The results for the second set of calculations are displayed in Fig. 8(a) and (b), respectively. Again, the performance ratios for the one-dimensional representation of the equivalent radial rectangular fin and the two-dimensional model with three different numbers of

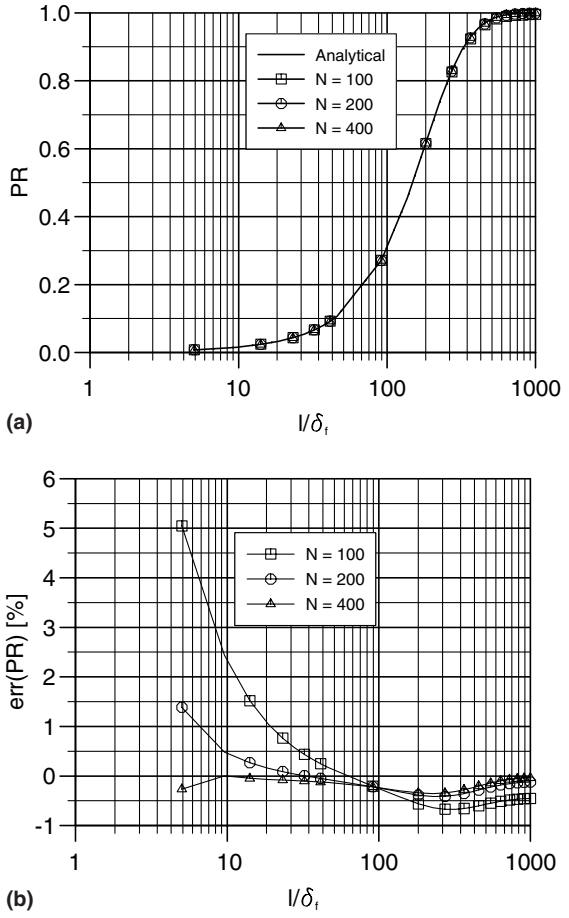

Fig. 7. (a) The analytical and the numerical values for the performance ratio PR, and (b) the error err(PR), as functions of l/δ_f, obtained for the square fin assembly with $\alpha = 20.0$ W m^{-2} K^{-1}, $\delta_f = 0.2 \times 10^{-3}$ m, $r_i = 7.0 \times 10^{-3}$ m, $\lambda_f = 202.4$ W m^{-1} K^{-1}, i.e. $\zeta_{max} = 224.50$ constant, $(T_b^2 - T_\infty)/(T_b^1 - T_\infty) = 0.90$ and $N \in \{100, 200, 400\}$ boundary elements.

boundary elements are plotted against the maximum effectiveness over the range illustrated in Fig. 5 by the horizontal dashed line. There appears to be excellent agreement between the one-dimensional approximation and the two-dimensional model over the full range. The percentage error given by Eq. (45) for the second set of results are plotted in Fig. 8(b) over the range of ζ_{max} values. Although not presented here, it is reported that similar results have been obtained for square fin assemblies with $\delta_f = 0.1 \times 10^{-3}$ m, as well as for various values of the ratio between the temperatures of the tubes, namely $(T_b^2 - T_\infty)/(T_b^1 - T_\infty) \in \{0.10, 0.50\}$.

In order to explain the results presented in Fig. 8(b), we have to account for the nature of the fundamental solution (33) for the modified Helmholtz equation and the role played by the maximum fin effectiveness, ζ_{max},

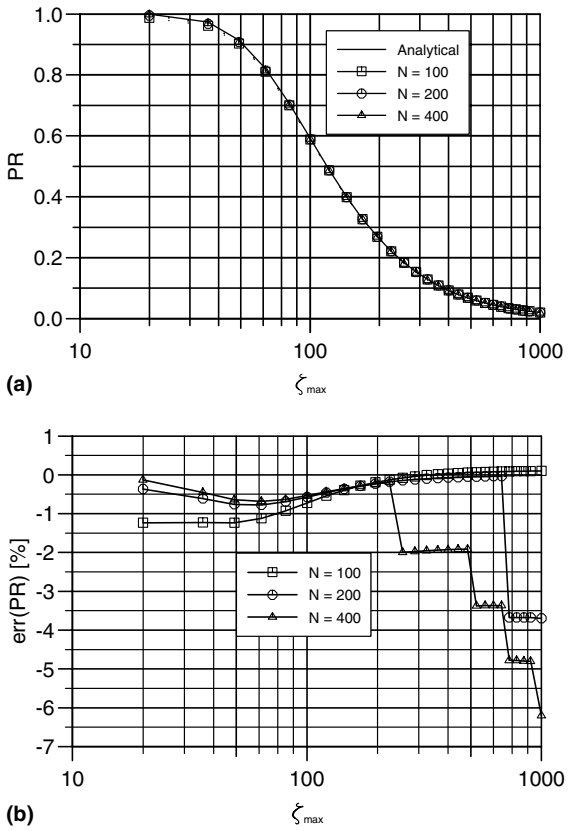

Fig. 8. (a) The analytical and the numerical values for the performance ratio PR, and (b) the error err(PR), as functions of ζ_{max}, obtained for the square fin assembly with $\alpha = 20.0\ \mathrm{W\,m^{-2}\,K^{-1}}$, $\delta_f = 0.2 \times 10^{-3}$ m, $r_i = 7.0 \times 10^{-3}$ m, $r_o^{(s)} = 28.49 \times 10^{-3}$ m, i.e. $l/\delta_f = 78.70$ constant, $(T_b^2 - T_\infty)/(T_b^1 - T_\infty) = 0.90$ and $N \in \{100, 200, 400\}$ boundary elements.

in the non-dimensionalisation process (4) of the governing equation (1) and the boundary conditions (2) and (3). Although for a fixed value of the reduced fin length, l/δ_f, i.e. the outer radius of the circle which encloses a single square fin, $r_o^{(s)}$, the inner radius (outer radius of the tube), r_i, and the fin length, δ_f, are fixed, the dimensions (geometry) of the domain occupied by the dimensional fin assembly do not change for various values of the maximum fin effectiveness, ζ_{max}, the geometrical non-dimensions of the domain occupied by the dimensionless model vary with respect to the maximum fin effectiveness, ζ_{max}, as can be noticed from Eqs. (8)–(13). For example, the values for the dimensionless outer radius of the circle which encloses a single square fin, $R_o^{(s)}$, and the inner radius, R_i, obtained with $\zeta_{max} \in \{224.50, 600, 1000\}$ are given by $R_o^{(s)} = 0.63$ and $R_i = 0.17$, $R_o^{(s)} = 0.23$ and $R_i = 0.05$, and $R_o^{(s)} = 0.11$ and $R_i = 0.03$, respectively. When using a large number of boundary elements to discretise the boundary of such domains, the distance, $r(\underline{X}^m, \underline{X}^n)$, from any collocation point, $\underline{X}^m$, to the midpoint, $\underline{X}^n$, of any boundary element has very small values and, in addition, $r(\underline{X}^m, \underline{X}^n) \approx r(\underline{X}^m, \underline{X}^{n+1})$. Since the modified Bessel functions of the second kind of orders zero and one, K_0 and K_1, respectively, have a strong singularity as the argument approaches zero, the integrals given by Eqs. (40) and (41) cannot be computed accurately in such cases. Hence it is expected that for large values of the maximum fin effectiveness, ζ_{max}, the use of $N = 200$ or $N = 400$ boundary elements to discretise the non-dimensional domain occupied by the square fin assembly will provide highly ill-conditioned BEM matrices and, therefore, the numerical results will deteriorate. It can be seen from Fig. 8(b) that the choice of the three BEM meshes with $N \in \{100, 200, 400\}$ is suitable for $\zeta_{max} \leqslant 170$, in the sense that the absolute value of the errors obtained using the aforementioned BEM discretisations decreases with respect to refining the mesh size. However, the errors obtained using $N \in \{100, 200, 400\}$ reach approximately the same value of about -0.30% for $\zeta_{max} = 170$ and this corresponds to a dimensionless domain characterised by $R_o^{(s)} = 0.83$ and $R_i = 0.20$. If the value for the maximum fin effectiveness becomes large, i.e. $\zeta_{max} \geqslant 675$ for $N = 200$ and $\zeta_{max} \geqslant 225$ for $N = 400$, and hence the boundary of the non-dimensionalised domain under investigation becomes small then the absolute value of the errors for the performance ratio numerically obtained using $N = 200$ and $N = 400$, respectively, starts increasing, as can be seen from Fig. 8(b). At the same time, the numerical results obtained for the fin performance ratio by discretising the boundary of the dimensionless domain with $N = 100$ elements are very accurate, i.e. $|\mathrm{err(PR)}| \leqslant 0.15\%$, showing that this mesh is sufficiently fine for such small domains. To summarise, in the case when the value of the reduced fin length, l/δ_f, is fixed and the maximum fin effectiveness, ζ_{max}, is varied, the finest BEM discretisation of the boundary corresponding to the domain occupied by the dimensionless fin assembly depends on the value of the maximum fin effectiveness considered, which is a parameter in the non-dimesionalisation process, and it should be chosen carefully such that the integrals given by Eqs. (40) and (41) can be computed accurately and the BEM matrices are not highly ill-conditioned.

Overall, from the numerical results presented and discussed in this section we can conclude that the BEM, in conjunction with the two-dimensional approach, provides very good estimates for the fin performance ratio for a polygonal fin assembly with two tubes on a square pitch and these are in a very good agreement with the results given by considering the design charts for the equivalent rectangular radial fin in the framework of the one-dimensional theory of heat flow along fins, see Figs. 4 and 5. However, the BEM mesh should be chosen carefully since it strongly depends upon the

geometrical dimensions and thermal conductivity of the fin assembly, as well as the coefficient of convective heat transfer, due to the nature of the fundamental solution for the modified Helmholtz equation and the role played by the maximum fin effectiveness in the non-dimensionalisation process of the governing partial differential equation. The agreement found between the two-dimensional theory and the equivalent one-dimensional radial rectangular representations means that the present design techniques, which use the concept of fin efficiency, are still acceptable. This occurs even though a two-dimensional fin efficiency definition does not exist.

7. Conclusions

A polygonal fin with two tubes arranged on a square pitch has been extensively analysed according to the two-dimensional theory. A semi-analytical solution has been obtained by the BEM and this solution is shown to be convergent, stable and consistent. This numerical method has increased accuracy due to the use of Green's integral identities and, furthermore, the solution function and its normal derivative at the boundary are simultaneously predicted. Only the boundary of the solution domain needs to be discretised, unlike the domain discretisation methods such as the finite-difference and finite element methods

The temperature distributions within the polygonal fin and the resultant heat flows to the surrounding air have been predicted for typical geometries and operating conditions in evaporators and condensers used in the refrigeration industry. The fin performance ratio concept has been used to present the two-dimensional temperature distributions and the heat flows. These values over a wide range of system parameters are shown to be almost identical to the analytical values obtained for a one-dimensional radial rectangular fin with the equivalent surface area of the polygonal fin and certainly well within engineering accuracy. Hence the heat flows can be predicted with confidence by the simple one-dimensional theory. Typical design charts are also presented for these predictions.

The two-dimensional analysis has also revealed the presence of conductive paths between the two tubes when there are significant temperature differences between the tubes. However, for this single fin, the heat flow to the surrounding air is identical to that predicted by the one-dimensional theory. The hotter tube exchanges more heat in the two-dimensional analysis, the additional heat compensates for the heat flow to the colder tube and provides the heat which the colder tube would have transferred. This is analogous to the so-called detrimental transverse conduction paths found in plate-fin heat exchangers, i.e. the half-fin assumption. Further studies detailing the two-dimensional analysis of polygonal fin assemblies with more than two tubes passing through them are on-going and they are approached using fast BEM procedures, such as the conjugate gradient method (CGM), see e.g. Golub and O'Leary [22] and the references therein.

Acknowledgement

The authors would like to acknowledge the financial support received from the EPSRC.

References

[1] L. Marin, L. Elliott, P.J. Heggs, D.B. Ingham, D. Lesnic, X. Wen, Analysis of polygonal fins using the boundary element method, Appl. Thermal Eng. 24 (2004) 1321–1339.
[2] A.D. Kraus, A. Aziz, J. Welty, Extended Surface Heat Transfer, McGraw-Hill, New York, 2001.
[3] K.A. Gardner, Efficiency of extended surface, Trans. ASME 67 (1945) 621–631.
[4] K.A. Gardner, Heat exchanger tube sheet temperatures, Refiner Nat. Gas. Mann. 21 (1942) 71–77.
[5] P.J. Heggs, Fin effectiveness is a better performance indicator than fin efficiency, in: IMechE, 6th UK National Conference on Heat Transfer, Edinburgh, 15–16 September 1999.
[6] P.J. Heggs, Fin heat transfer: 80 years since Harper and Brown's paper—What is new? The fin performance ratio, in: Proceeding of the 2nd World Engineering Congress, Engineering Innovation and Sustainability: Global Challenges and Issues, Sarwak, Malaysia, 22–25 July 2002.
[7] D.R. Harper, W.B. Brown, Mathematical equations for heat conduction in the fins of air-cooled engines, NACA Report no. 158, 1922.
[8] I. Mikk, Convective fin of minimum mass, Int. J. Heat Mass Transfer 23 (1980) 707–711.
[9] R.K. Irey, Errors in the one-dimensional fin solution, J. Heat Transfer 90 (1968) 175–176.
[10] M. Levitsky, The criterion for the validity of the fin approximation, Int. J. Heat Mass Transfer 15 (1972) 1960–1963.
[11] W. Lau, C.W. Tan, Errors in one-dimensional heat transfer analysis in straight and annular fins, J. Heat Transfer 95 (1973) 549–551.
[12] E.M. Sparrow, L. Lee, Effects of fin base-temperature depression in a multi-fin array, J. Heat Transfer 97 (1975) 463–465.
[13] N.V. Suryanarayana, Two-dimensional effects on heat transfer rates from an array of straight fins, J. Heat Transfer 99 (1977) 129–132.
[14] P.J. Heggs, P.R. Stones, The effects of dimensions on the heat flow rate through extended surfaces, J. Heat Transfer 102 (1980) 180–182.
[15] F.P. Incropera, D.P. DeWitt, Fundamentals of Heat and Mass Transfer, Wiley, New York, 1990.
[16] P.J. Heggs, T.H. Ooi, Design charts for radial rectangular fins in terms of performance ratio and maximum fin effectiveness, Appl. Thermal Eng. 24 (2004) 1341–1351.

[17] G. Chen, J. Zhou, Boundary Element Methods, Academic Press, London, 1992.
[18] Z.H. Rizvi, Design methodology for refrigeration and air conditioning systems, Ph.D. Thesis, UMIST, 2001.
[19] A. Ralston, A First Course in Numerical Analysis, McGraw-Hill, New York, 1965.
[20] B.S.V. Prasad, Fin efficiency and mechanisms of heat exchange through fins in multistream plate-fin heat exchangers: Formulation, Int. J. Heat Mass Transfer 39 (1996) 419–428.
[21] W.O. de Geraldelli, Design methodology and mathematical modelling of multistream plate-fin heat exchangers, Ph.D. Thesis, UMIST, 2001.
[22] G.H. Golub, D.P. O'Leary, Some history of the conjugate gradient and Lanczos algorithms: 1948–1976, SIAM Rev. 31 (1989) 50–102.